Nanomechanical behavior of MoS$_2$ and WS$_2$ multi-walled nanotubes and Carbon nanohorns

Dave Maharaj & Bharat Bhushan

Nanoprobe Laboratory for Bio-& Nanotechnology and Biomimetics (NLBB), The Ohio State University, 201 W.19th Avenue Columbus, Ohio 43210-1142, USA.

Nano-objects have been investigated for drug delivery, oil detection, contaminant removal, and tribology applications. In some applications, they are subjected to friction and deformation during contact with each other and their surfaces on which they slide. Experimental studies directly comparing local and global deformation are lacking. This research performs nanoindentation (local deformation) and compression tests (global deformation) with a nanoindenter (sharp tip and flat punch, respectively) on molybdenum disulfide (MoS$_2$) multi-walled nanotubes (MWNTs), $\sim$500 nm in diameter. Hardness of the MoS$_2$ nanotube was similar to bulk and does not follow the "smaller is stronger" phenomenon as previously reported for other nano-objects. Tungsten disulfide (WS$_2$) MWNTs, $\sim$300 nm in diameter and carbon nanohorns (CNHs) 80–100 nm in diameter were of interest and also selected for compression studies. These studies aid in understanding the mechanisms involved during global deformation when nano-objects are introduced to reduce friction and wear. For compression, highest loads were required for WS$_2$ nanotubes, then MoS$_2$ nanotubes and CNHs to achieve the same displacement. This was due to the greater number of defects with the MoS$_2$ nanotubes and the flexibility of the CNHs. Repeat compression tests of nano-objects were performed showing a hardening effect for all three nano-objects.

N ano-objects have been investigated for applications that include drug delivery for cancer treatment, oil detection, contaminant removal and tribology on the macro- to nanoscale. In some applications, they are subjected to friction and deformation during contact with each other and the surfaces on which they are used. The nano-objects can be deformed locally where they may be indented, or globally where the entire nano-object is compressed. To determine their suitability for applications, fundamental understanding of interfacial friction and wear, their mechanical properties and deformation mechanisms is needed.

In targeted drug delivery applications, Au, Fe$_2$O$_3$, polymer and SiO$_2$ nano-objects have been studied[1–4]. For applications requiring chemical sensors, oxidized carbon black coated with oil detecting agents and composites of collagen and iron oxide nanoparticles have been used[5–8]. In contaminant removal, magnetic shell cross-linked knedel-like nanoparticles (MSCKs) are of interest[9]. In tribological applications on the macro-to nanoscale, a large body of data exists on nano-objects and examples of materials are given along with the various studies. Nanoparticles including Au, CNHs, Fe$_2$O$_3$, Sb, MoS$_2$ and WS$_2$; nanorods including ZnS, ZnO and AgVO$_3$; and nanotubes including MoS$_2$, WS$_2$, and CNT have been used. Studies have been carried out on the macro-scale[10–17], microscale[18–20] and nanoscale[15–17,21–28].

In many applications described, low friction and wear is desirable for efficient and sustained use. The nano-objects may come into sliding contact with each other and the surfaces in which they are used. During sliding contact, asperities present on the mating surfaces come into contact and deform, to support the load. Adhesive contacts are formed with the asperities by either physical or chemical interactions. When the surfaces move relative to each other a shear force is needed to break the adhesive bonds formed at the real area of contact. The friction measured is given as: Real area of contact is directly related to the nanomechanical properties relevant to nanoscale asperity contacts.

$$F = A_r \tau \qquad (1)$$

where A_r is the real area of contact and τ is the average shear strength of the contacts[30]. Both reduction in shear strength and contact area reduces friction as well as wear. Deformation of nano-objects increases the real area of contact and causes friction and wear to increase.

For friction and wear reduction on the macro- to nanoscle, nano-objects made of MoS_2, WS_2 and graphene are of interest. In tribology, MoS_2 and WS_2 coatings and nano-objects have been used due to their ability to reduce the real area of contact between sliding surfaces and reduce friction and wear. Nanotubes made of these materials can also reduce friction and wear through rolling, sliding and exfoliation of the outer layers (peeling of layers) to form a tribofilm on the macro – to nanoscale[16,28]. Nano-objects made of graphene such as CNHs have also been used for friction reduction on the macro – to nanoscale. The additional roughness provided by the nanohorns can further reduce the contact area in addition to rolling and sliding[17].

Understanding the mechanical behavior of MoS_2 and WS_2 MWNTs and CNHs under varying loading conditions during sliding is important for friction and wear reduction. Previous compression studies on MoS_2 and WS_2 nanoparticles have been performed using a nanomanipulator with an AFM probe[26–27]. Lahouji et al[26]. suggested rolling, sliding and exfoliation (peeling of layers) of an IF-MoS_2 nano-object, as the AFM probe was translated over it in dry conditions. These experiments were performed inside of a transmission electron microscopy (TEM) chamber. Tevet et al[27]. also suggested rolling, sliding and exfoliation of IF-WS_2 and MoS_2 nanoparticles inside of a high resolution scanning electron microscopy (HRSEM) chamber. They were also able to show that each mechanism takes place under different loading regimes. Studies that directly compare indentation (local deformation) and compression (global deformation) have been performed on Au nanoparticles (500 nm)[29]. Similar studies on other nano-objects have not been performed. Given the importance of MoS_2 and WS_2 MWNTs and CNHs in friction and wear reduction under various loading conditions, additional studies on deformation mechanisms of these nano-objects are needed.

In this study, MoS_2 and WS_2 MWNTs and CNHs were investigated to determine their mechanical behavior. Nanoscale measurements were made to study scale effects. By using a sharp tip and a flat punch, local deformation (indentation) and global deformation (compression) behavior were studied. Repeat compression tests of all three nano-objects were performed to study nanoscale hardening.

Methods

Mechanical behavior under local deformation (indentation) with a sharp tip and global deformation (compression) with a flat punch were studied. MoS_2 and WS_2 MWNTs and CNHs nano-objects were selected because of their ability to reduce friction and wear. It is important to understand their mechanical behavior under different loading conditions that simulate the environments in which they may be used.

The nominal diameters of MoS_2 MWNTs were ~500 nm with lengths of 15–20 μm and for WS_2 MWNTs the nominal diameters were ~300 nm and also 15–20 μm in length. The CNHs comprise of horn shaped sheets of single-walled graphene 2–3 nm in diameter with a length of 30–50 nm. These horns, aggregate to form nanoparticles with nominal diameters of 80–100 nm.

For the determination of mechanical properties and scale effects compared to bulk, the MoS_2 MWNTs ~500 nm in diameter were selected. The large diameter of the nanotubes compared to the 100 nm radius of the sharp tip provides a flatter surface for nanoindentation compared to the other nano-objects. This allows for reduction of curvature effects. As nano-object size decreases there is less contact with the tip due to the curvature of both the tip and nano-object and this can lead to inaccurate determination of contact area. This results in errors in obtaining mechanical properties accurately. In determination of mechanical properties a displacement of 50 nm was selected. This was done to obtain well defined load-displacement curves where the contact depth does not exceed 30% of the nano-object thickness and result in sub-strate hardening effects[31].

Compression studies were also performed on the MoS_2 MWNTs to compare local and global deformation. Compression studies of WS_2 MWNTs and CNHs to observe mechanical behavior during global deformation were also performed along with repeat compression tests to study nanoscale hardening. Further details are given in the section on nanomechanical characterization for indentation and compression.

Materials and Sample preparation. Si (100) silicon wafers with a native oxide layer (University Wafers, Boston, MA) were ultrasonically cleaned in deionized (DI) water, followed by isopropyl alcohol (IPA) and finally acetone for 15 min each.

Figure 1 shows representative images of the nanotubes and nanoparticles used for the experiments performed. MoS_2 nanotubes were obtained from Josef Stefan Institute, Ljubljana, Slovenia and WS_2 nanotubes from Weizmann Institute, Rehovot, Israel and were manufactured as discussed by Maharaj and Bhushan[16]. Figure 1a

shows representative transmission electron microscopy (TEM) micrographs of a MoS_2 nanotube with a broken edge (Top), a magnified image showing separated layers between the arrows (Left), magnified image showing broken surface layers (Center) and a magnified image of a nanotube showing stacking faults highlighted by the dashed lines (Right). Figure 1b shows agglomerated WS_2 nanotubes (Left), a magnified image with an arrow pointing to exfoliated layers (Center) and a magnified image of a nanotube showing ordered layers. Single-walled graphitic CNHs (Meijo University, Japan) were created as described by Iijima et al[32]. and Kasuya et al[33]. CNHs are spherical nano-objects made of single layers of graphene in the shape of horns. The horns agglomerate through van der Waals attraction to form the nano-object. Figure 1c shows TEM micrographs of spherical CNHs (Left) with a magnified image of CNHs (center) and a magnified image of individual nanohorns (Right)[32].

CNHs added to ethanol and MoS_2 and WS_2 nanotubes added to isopropyl alcohol (IPA) were sonicated for an hour to disperse the nano-objects. For experiments involving nano-object coated surfaces in dry conditions, several droplets of MoS_2 and WS_2 nanotubes suspended in IPA and CNHs suspended in ethanol, were deposited onto clean Si (100) substrates using a syringe. A solution concentration of 0.01 mg/ml was used. The substrate was then placed on a hot plate and heated to a temperature of about 70–80°C and left until the liquid evaporated. For the micrographs the nano-objects are deposited on a lacey carbon support (Ted Pella, Redding, CA) and then placed in a holder and observed using a TEM system (Tecnai F20, FEI, Hillsboro, OR) operated at a voltage of 200 kV with a current of 1nA.
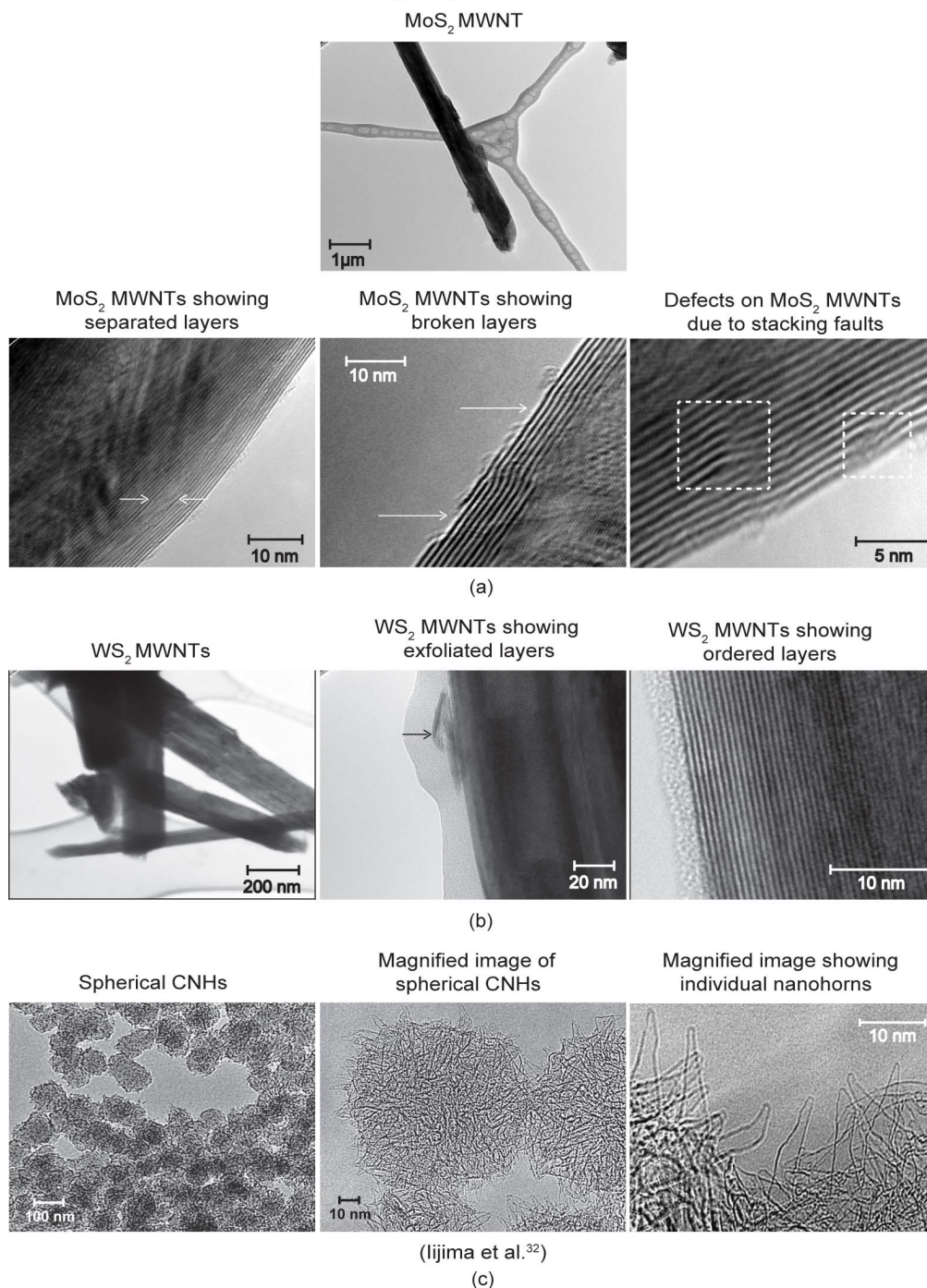
Nanomechanical characterization- *Nanoindentation*. All experiments were carried out using a probe based scanning nanoindenter head TS 75 Trboscope, (Hysitron, Inc., Minneapolis, MN) attached to an AFM (Dimension 3100, Bruker, Santa Barbara, CA) with a diamond tip.

For nanoindentation experiments a three-sided diamond pyramidal Berkovich tip of approximately 100 nm in radius was used as shown in Figure 2 (left). These experiments were only performed on the 500 nm diameter MoS_2 nanotubes. It is necessary to provide as flat a surface as possible for nanoindentation. This allows for elimination of curvature effects and more accurate determination of the contact area and mechanical properties. This was not possible with the other nano-objects due to their smaller dimensions. Hardness and elastic modulus were obtained by indenting at maximum displacement of 50 nm perpendicular to the basal plane. This was done to obtain well defined load-displacement curves where the contact depth does not exceed 30% of the nano-object thickness and result in substrate hardening effects[31]. Displacements of 100 nm were also explored and were the maximum displacements possible before the Berkovich tip penetrated the walls of the nanotube into the hollow interior. This was done to explore deformation under increased depths of penetration.

The Oliver and Pharr[34] method was used to obtain the hardness and elastic modulus of MoS_2 nanotube. A reduced modulus is obtained from the slope of the unloading part of the load-displacement curve. This is a function of the Young's moduli and Poisson's ratios of diamond and MoS_2. The Young's modulus of elasticity and Poisson's ratio for diamond were taken as 1141 GPa and 0.07 respectively[35]. Poisson's ratio for MoS_2 was taken as 0.27[36]. The unknown Young's modulus of MoS_2 can now be determined. Hardness is found from the ratio of the maximum load to the contact area. The data from these experiments is the average of five measurements on five different nanotubes for each load. The duration for loading and unloading was 20 s for all experiments (unless otherwise stated) to safeguard against the nanotube slipping under the indenter during more rapid and unstable loading. Topography images were also taken before and after indentation with the same tip used for indentation. All experiments were performed at room temperature (23°C) and 50–55% relative humidity.

Nanomechanical characterization- *Compression*. For compression experiments a spherical diamond tip of approximately 3.5 μm in radius was used as shown in Figure 2 (right). This can be considered to be a flat punch due to the large radius of the diamond tip compared to the nano-objects. Compression was performed under displacement control for displacements of 50, 100 and 300 nm for the MoS_2 MWNTs. These displacements were selected to understand how the nano-objects deform under various levels of compression. The lowest displacement was 50 nm similar to indentation. This was done to compare the deformation between indentation and compression and to investigate global deformation for MoS_2, WS_2 MWNTs and CNHs. For the CNHs displacements were 25, 50 and 75 nm due to smaller diameters of the nanoparticles which ranged from 80–100 nm. Repeat compression loading experiments, where the nano-objects are loaded several times for a fixed displacement, were performed. Experiments were carried out to explore hardening effects on the nanoscale as well as pop-in behavior. For the nanotubes the displacement was held constant at 50 nm. The number of compressions was limited by the nanotubes either being pushed during imaging or stuck to the diamond tip during compression. This makes imaging and location of the nanotube impossible for further compression. For the CNHs the displacement was held constant at 25 nm. The duration for loading and unloading was 20 s for all experiments similar to nanoindentation. Topography images were also taken before and after indentation with the same tip used for compression.

To ensure repeatability, each experiment was performed five times and representative data are shown in the results section. Experiments were performed at room temperature (23°C) and 50–55% relative humidity for the nanotubes and for the CNHs the relative humidity was 70–75% to ensure that the nanoparticles were securely held in place by adhesive meniscus forces due to its lubricious nature.

TEM of MoS$_2$, WS$_2$ and CNH nano-objects

MoS$_2$ MWNT

MoS$_2$ MWNTs showing separated layers | MoS$_2$ MWNTs showing broken layers | Defects on MoS$_2$ MWNTs due to stacking faults

(a)

WS$_2$ MWNTs | WS$_2$ MWNTs showing exfoliated layers | WS$_2$ MWNTs showing ordered layers

(b)

Spherical CNHs | Magnified image of spherical CNHs | Magnified image showing individual nanohorns

(Iijima et al.[32])

(c)

Figure 1 | TEM images of (a) MoS$_2$ MWNT (Top), a magnified image showing separated layers between the arrows (Left), magnified image showing broken surface layers (Center) and a magnified image of a nanotube showing stacking faults highlighted by the dashed lines (Right) (b) agglomerated WS$_2$ MWNTS (Left), a magnified image with an arrow pointing to exfoliated layers (Center) and a magnified image of a nanotube showing ordered layers. (c) Spherical CNHs (Left) with magnified image of CNHs (Right) (Iijima et al., 1999).

Mechanism. In order to understand the data presented for MoS$_2$ MWNTs and WS$_2$ MWNTs and explain mechanical behavior during deformation, it is important to provide a detailed explanation of the underlying mechanisms involved.

It is known that movement of dislocations by slip causes plastic deformation to occur. In lamellar structures as found in MoS$_2$ and WS$_2$, stacking faults that are created during material formation are accompanied by partial dislocations. Local regions in a crystal consist of layers of atoms on top of each other in a repeating pattern known as the stacking order. The first layer is designated as the 'A' layer and successive layers are given a new letter designation such as 'B' or 'C' if offset to the original layer and each other. Stacking faults results when this order is interrupted by

either introduction or removal of an extra plane of atoms as shown in Figure 3[37]. Where the fault ends within the crystal, the area separating the faulted region from the perfect crystal is a partial dislocation. Figure 3 illustrates the concept of stacking faults and partial dislocations with Frank and Shockley partials.

Frank partials are sessile and do not move by dislocation slip and prevents plastic deformation by obstructing movement of dislocations that can slide. Figure 3a shows an example, where a plane of atoms are missing within a layer of atoms with 'A to A' arrangement. The plane of atoms above and below, shift and settle into the vacant area. It is energetically unstable to have two layers of atoms with similar arrangement stacked on top of each other. To return to a more stable state, the internal arrange-

Method of deformation
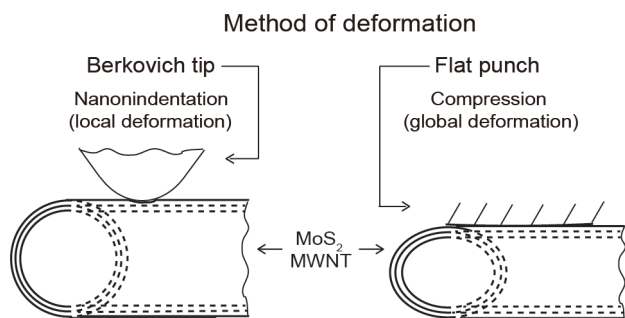
Figure 2 | Schematic showing method of deformation using a Berkovich tip for nanoindentation (local deformation) and flat punch for compression (global deformation) with MoS₂ MWNTs as an example.

ment of atoms above the missing layer changes from a 'B to B' to a 'B to C' configuration. This causes subsequent internal layers above it, to also rearrange themselves to accommodate this change. Figure 3b shows a stacking fault resulting from a Shockley partial as an example. This results in a stacking fault where a 'C' arrangement of atoms is found within an 'A' layer shown within the dashed lines. In this case the 'C' arrangement is preferred to one with 'B' since it is more energetically favorable. Shockley partials are glissile and move leading to slip and plastic deformation[37].

Results and Discussion

Results for nanoindentation using a Berkovich tip and compression using a flat punch are given for MoS₂ MWNTs and only compression for WS₂ MWNTs and CNHs. For both deformation methods, representative load-displacement curves are presented. Morphological characterization, before and after deformation, is also presented using a Berkovich tip. Finally load-displacement curves for repeat compression tests using the flat punch are presented.

Nanomechanical characterization- *Nanoindentation.* Indentation with a Berkovich tip was used to determine the mechanical properties of MoS₂ MWNTs. This was done using displacement control at a maximum displacement of 50 nm. Figure 4a shows a typical load-displacement curve with topography maps of the MWNTs over a 20 μm × 20 μm scan area and 2-D profiles before and after indentation. The topography maps are used to confirm the indentation of the nanotubes and that the nanotube did not slip during loading and unloading. The vertical arrows on the load-

displacement curves point to pop-in events during indentation. The horizontal white arrows indicate the nanotube of interest along with the section on which the profiles were taken. The indent is highlighted by the dashed square on the "after indentation" profile and is not present on the "before indentation profile" at the same location.

Pop-ins have been observed in metallic and intermetallic materials by Göken and Kempf[38] during initial steps of loading. They were reported to represent a sharp transition from pure elastic loading to a plastic deformation corresponding to an initial yield point. In the experiments with nanotubes pop-ins are believed to be as a result of displacement during breaking of the individual layers as well as sudden displacement through the spaces between the separated layers and already broken layers as shown in Figure 1a (Left and center). Figure 3a–b shows stacking faults where Frank and Shockley partial dislocations form at the edge of the fault. Since the Frank partials increase resistance to deformation, the breaking of the layers through plastic deformation occurs due to slip of Shockley partial dislocations which causes plastic deformation.

The hardness and Young's modulus were found at a displacement of 50 nm normal to the basal plane and are given in Table 1. The hardness and Young's modulus for MoS₂ MWNTs was found to be 0.6 GPa ± 0.2 GPa and 12.5 GPa ± 4 GPa respectively. Bulk MoS₂ has a similar hardness (0.6 GPa) and a Young's modulus of 52 GPa normal to the basal plane. This was determined by Feldman[36] based on neutron data by Wakabayashi et al[41]. of a 2 mm thick MoS₂ crystal. The lower Young's modulus of the MoS₂ MWNTs occurs as a result of the broken and separated layers present in the nanotube walls which provide less resistance to deformation (Figure 1a). The hardness of the MoS₂ nanotube does not follow the smaller is stronger phenomenon seen in various nano-objects made of materials including Au, Cu, Nb and Ni[29,42-47].

In studies, for polycrystalline nano-objects, the grain sizes were smaller than those found in bulk, which leads to dislocation pile-ups and an increased density of dislocations which entangle and resists plastic deformation[48–52]. In the case of single crystalline nano-objects, dislocation starvation occurs where the absence of dislocations in the interior of the nano-object limits plastic deformation[43]. The thin layers that comprise the walls of the MoS₂ nanotubes are single crystalline and mechanisms associated with grain sizes are not relevant. Dislocation starvation is also not possible since stacking faults are observed in Figure 1a (Right) and both Frank and Shockley

Illustration of stacking faults with Frank and Shockley partial dislocations
(Based on Hull and Bacon, 2001)
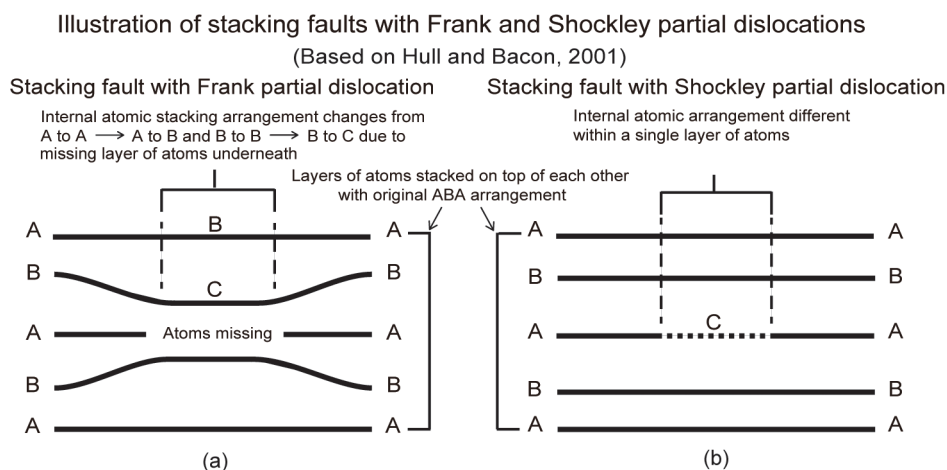
Figure 3 | Schematic showing (a) stacking faults resulting from the removal of a plane of atoms with sessile Frank partials dislocations in the region between the faulted and perfect crystal. The layer directly above the missing atoms changes internally from a 'B to B' to 'B to C' arrangement to prevent an energetically unstable arrangement (Hull and Bacon, 2001). The subsequent layer changes from an 'A to A' to 'A to B' arrangement, and (b) stacking faults with glissile Shockley partials in the region between the faulted and perfect crystal. These faults are as a result of an insertion of a plane of atoms with 'C' arrangement between a layer with 'A' arrangement. The 'C' arrangement is more energetically favorable to a 'B' arrangement.
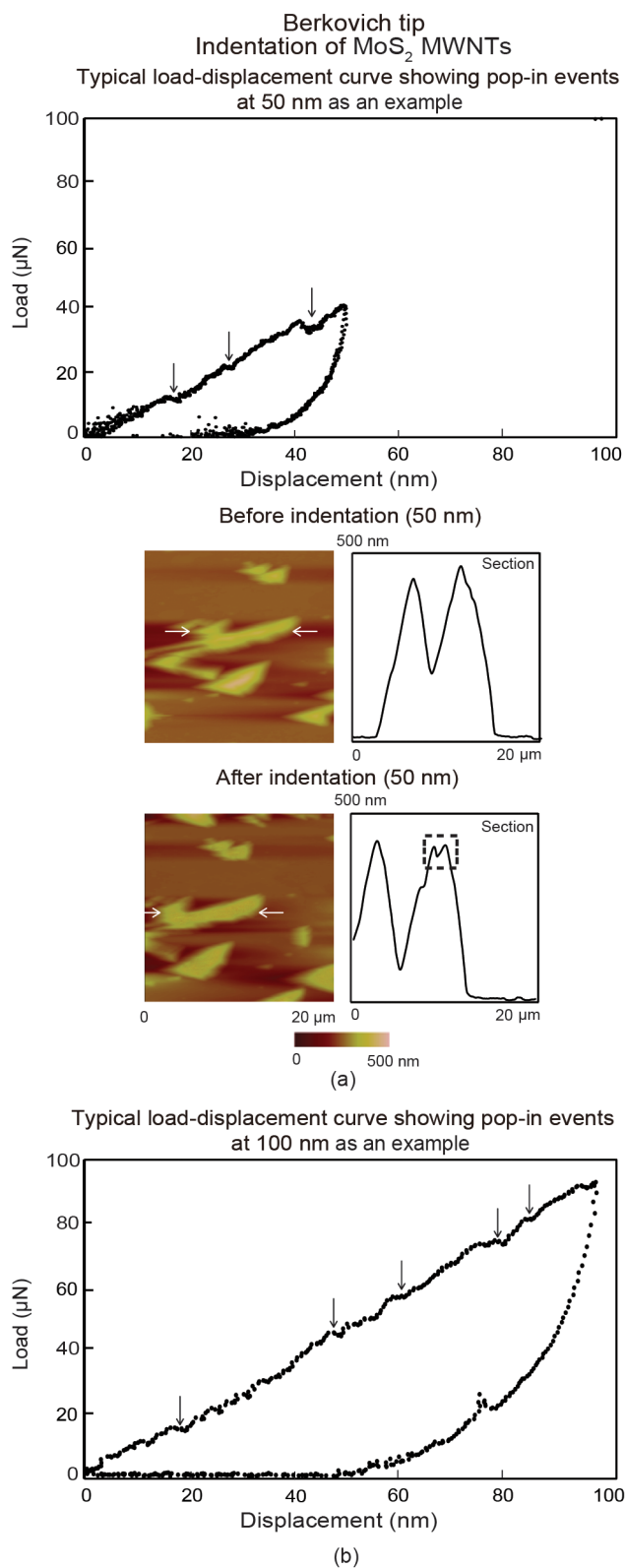
Figure 4 | (a) Typical load-displacement curve for low displacement of 50 nm for MoS$_2$ MWNTs and topography maps and 2-D profiles, at sections indicated by the horizontal arrows before indentation (first row) and after indentation (second row). The dashed square highlights the indent in the "after indentation profile" (b) Typical load-displacement curve for high displacement of 100 nm. Vertical arrows point to pop-in events for both curves which occur due breaking of nanotube layers and sudden compression of separated layers. Indentation was performed on separate nanotubes for low and high displacement.

partial dislocations are present. In this case, separated layers, broken layers, and missing layers and Shockley dislocations decrease resistance to deformation and compete with Frank dislocations present which increase resistance to deformation, as explained previously in the mechanism section. These competing effects result in no appreciable increase in hardness.

To further understand deformation during indentation, higher displacements were also explored. Figure 4b shows indentation at a displacement close to 100 nm with a larger number of pop-ins compared to displacement of 50 nm. This is due to a greater number of defects, such as broken, separated and missing layers, encountered by the diamond tip as the layers are penetrated.

The broken and separated layers can lead to exfoliation as the layers are easier to peel apart at higher loads. In applications requiring friction and wear reduction this can be beneficial as exfoliation leads to formation of an easily sheared film which leads to lower friction and wear[16,17].

In summary, the load-displacement curves for MoS$_2$ MWNTs revealed several pop-in effects which result from slip as the sharp tip penetrates broken layers and spaces between separated layers. No scale effects were observed. Separated layers, broken layers, and missing layers and Shockley dislocations decrease resistance to deformation and compete with Frank dislocations present which increase resistance to deformation. These competing effects result in no appreciable increase in hardness.

Nanomechanical characterization- *Compression*. Nano-objects were compressed to understand global deformation (compression) behavior and compare to local deformation (indentation). For this purpose, a tip approximately 3.5 μm in radius was used to carry out compression tests. Compression data for the MWNTs are presented first, followed by CNHs.

Figure 5 shows typical load displacement curves for compression at maximum displacements of 50, 100 and 300 nm for MoS$_2$ and WS$_2$ MWNTs. The vertical arrows point to some examples of pop-in events during compression of the nanotubes. These events similar to indentation are a result of breaking of the layers of the walls of the MoS$_2$ and WS$_2$ nanotubes where plastic deformation occurs as a result of slip of Shockley partial dislocations. In the case of MoS$_2$ nanotubes, compression of spaces between separated layers also contributes to pop-ins. For the MoS$_2$ MWNTs there are less pop-in events during compression compared to indentation (Figure 4). Here, the entire nanotube is compressed and there is more resistance to deformation and breaking of the layers of the nanotube walls. For WS$_2$ MWNTs, a greater load is required for the same displacement (50 nm) as compared to MoS$_2$ MWNTs. At a depth as low as 50 nm, hardening due to substrate effects are unlikely as the displacement is less than 30%[31] of the height of the nanotubes. The higher resistance to deformation of the WS$_2$ MWNTs, is due to fewer defects (Figure 1b), as there are no separated layers or broken layers present as in the case of MoS$_2$ MWNTs. However, even though there are more pop-ins at higher displacement s (100 nm and 300 nm) for MoS$_2$ MWNTs the difference in load between the MoS$_2$ and WS$_2$ MWNTS is less as the substrate begins to influence the resistance to deformation and creates a hardening effect.

The broken layers of MoS$_2$ MWNTS shown in Figure 1a (Center) and can lead to exfoliation as the layers come apart under increasing load. This along with already exfoliated layers (center) on WS$_2$ MWNTs as shown in Figure 1b (Center) can lead to formation of an easily shearable film during sliding in tribological applications, which reduces friction and wear. For WS$_2$ MWNTs, greater resistance to compression can also be beneficial for reduction of friction and wear. In instances where there is high moisture content, MoO$_3$ and WO$_3$ can be formed as MoS$_2$ and WS$_2$ become oxidized in the presence of oxygen. In these situations the film formation is interrupted as layers clump together. The water vapor present can also

Table 1 | Mechanical properties of MoS₂ MWNTs obtained from the nanoindentation experiments normal to the basal plane. For comparison, mechanical properties of naturally occurring MoS₂ (normal to the basal planes) and single layer graphene are given

Mechanical Properties	MoS$_2$ MWNts (500 nm)	MoS$_2$[10,36] (2 mm)	Graphene[39,40] (single layer)
Young's modulus (GPa)	12.5 ± 4	52	1000
Hardness (GPa)	0.6 ± 0.2	0.6	950

condense in the defects of the crystal structure as shown in Figure 1a, b and would interrupt the easy shear of the basal planes[53–55]. Since the WS₂ MWNTs offer better resistance to deformation compared to the MoS₂ MWNTs, these may be more suitable for friction and wear reduction in humid conditions. In this case since the nanotube layers are not as easily exfoliated, the friction and wear reduction is as a result of reduced contact area, sliding and possible rolling[16,17].

Compression data for CNHs are now presented and compared to the MWNTs. Figure 6 shows load-displacement compression curves for CNHs for displacements of 25, 50 and 75 nm with vertical arrows pointing to pop-in events. Lower displacements were chosen for the compression due to the smaller diameter of the nanoparticles (80–100 nm). Similar to the MoS₂ and WS₂ MWNTs, pop-in events occur with CNHs at all three displacements. The single layer
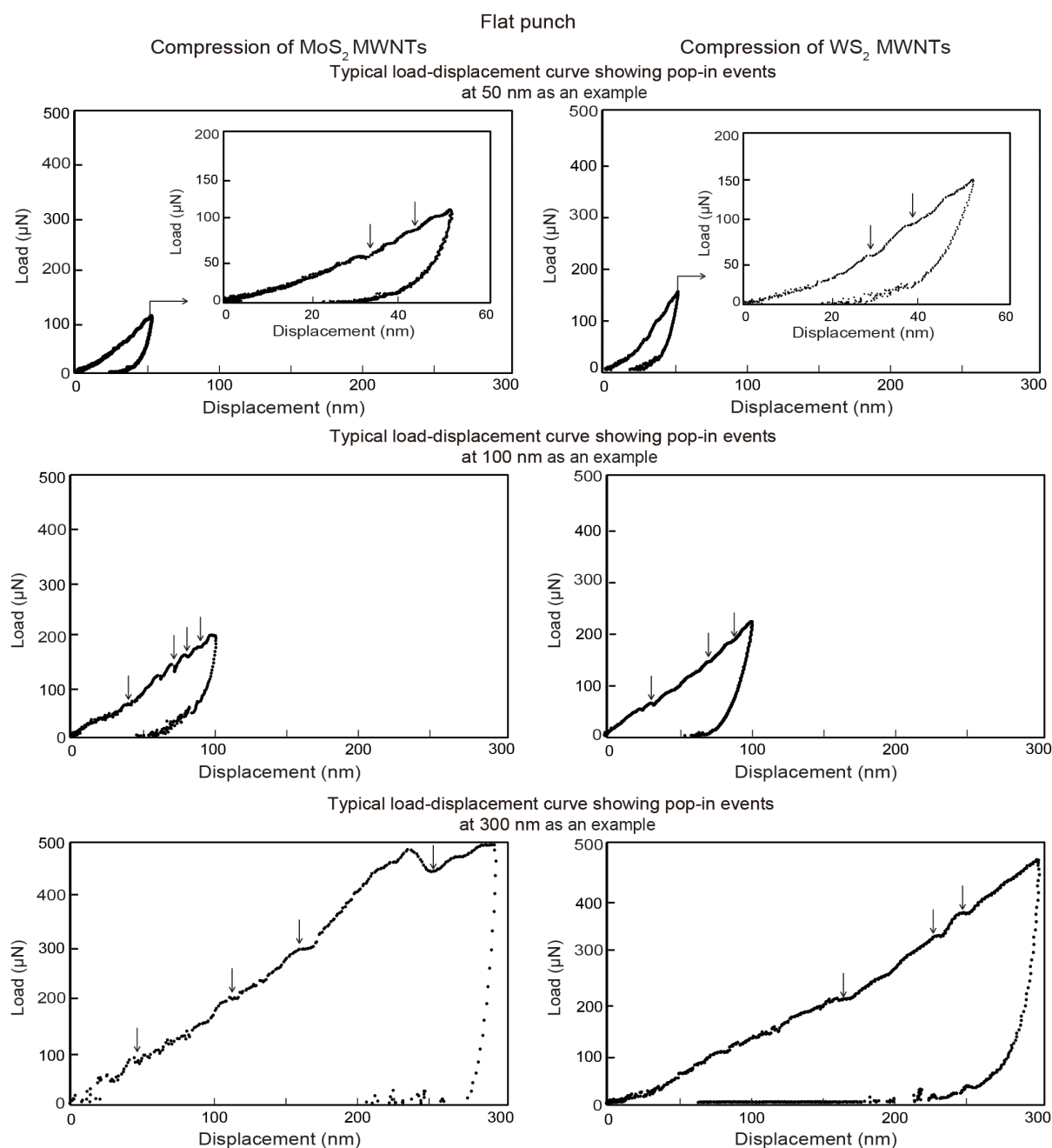
Figure 5 | Compression load displacement curves for displacements of 50 nm, 100 nm and 300 nm for MoS₂ (Left) and WS₂ MWNTs (Right) with the vertical arrows depicting pop-in events. Magnified images are shown inset for displacements of 50 nm to more clearly illustrate pop-in events which are a result of breaking of individual layers of the nanotubes and sudden compression of separated layers.

graphene horns which comprise CNHs, have a high hardness of 950 GPa and Young's modulus of 1000 GPa as shown in Table 1, but at the same time is very flexible and can easily bend[56]. The pop-ins for CNHs occurs as a result of buckling of the individual nano-horns. For a displacement of 50 nm a lower load (80 μN) for the CNHs is required to produce the same displacement compared the MoS_2 and WS_2 MWNTs, shown in Figure 5 (108 μN and 150 μN), due to the flexibility of the CNHs.

For tribological applications under high loads, rolling and sliding of spherical CNHs may not be possible due to their flexible nature and ability to deform easily. The individual nanohorns can still reduce friction and wear since they will not break apart easily due to the high hardness and Young's modulus and would provide an easily shearable layer for sliding which would reduce friction and wear. In summary, MoS_2 and WS_2 MWNTs and CNHs, pop-ins are observed under low to high displacements. The mechanism for the MWNTs is different from the CNHs, where the individual walls breaks compared to buckling of the individual nanohorns which are flexible. This flexibility was further seen where, for a comparable displacement for all three nano-objects, CNHs required the lowest load. Further compression tests to study hardening effects of the nano-objects were also performed.

Repeat compression tests were performed at a constant displacement of 50 nm for the MoS_2 and WS_2 MWNTs and 25 nm for the CNHs. This provides an opportunity to study hardening effects on the nanoscale. Figure 7 shows load displacement curves for repeat compression for the nano-objects. For all cases higher consecutive loads are required to produce the same displacements. This depicts a hardening effect up to the loads used. The layers of the MoS_2 and WS_2 nanotube walls are pressed together and the spaces between them become smaller. As they are pressed into the substrate a higher load is required to produce the same displacement for each successive run. The vertical arrows point to examples of pop-ins as individual layers that comprise the nanotube walls break. For the CNHs, as individuals nanohorns buckle and are pressed onto each other and the substrate, further compression becomes more difficult, similar to the MWNTs. Pop-ins in this case occur due to buckling of the individual nanohorns.

In summary, all three nano-objects display pop-in effects during loading and increased resistance to deformation during repeat compression tests. CNHs required the smallest load for a displacement of 50 nm compared to the MWNTs. This is due to buckling of the individual nanohorns as a result of their flexible nature.

The increased resistance to deformation with the repeat compression can be useful in situations where repeated contacts occur in tribological systems on the macro- to nanoscale as deformation of the nano-objects becomes more difficult.

Conclusions

MoS_2 (500 nm in diameter) and WS_2 MWNTs (300 nm in diameter) and CNHs (80–100 nm in diameter) were investigated to determine their mechanical behavior. MoS_2 MWNTs were investigated to study scale effects and local deformation (nanoindentation) with a sharp tip. Nanoindentation was performed only on the MoS_2 MWNTs. Since decreasing nano-object size results in less contact with the tip due to the curvature of both the tip and nano-object this can lead to inaccuracies in determining contact area, consequently mechanical properties. The large diameter of the MoS_2 MWNTs provides a flatter surface for nanoindentation compared to the other nano-objects and leads to less error in determination of mechanical properties. Global deformation (compression) studies were performed on all samples including MoS_2 and WS_2 MWNTs and CNHs with a flat punch using a depth sensing nanoindenter in order to compare mechanical behavior during both types of deformation. This was carried out displacements from low to high. Hardening was investigated by compression using repeat loads.

Flat punch
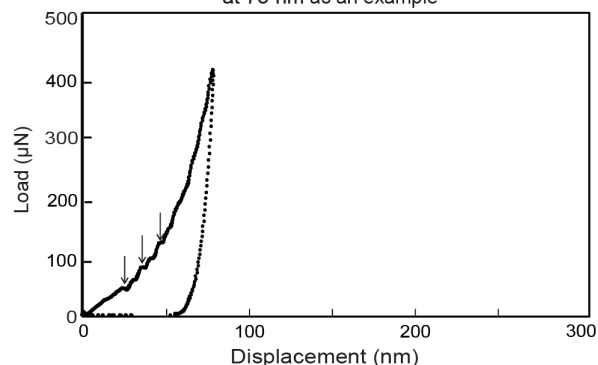Compression of CNH with Displacement of 25, 50 and 75 nm
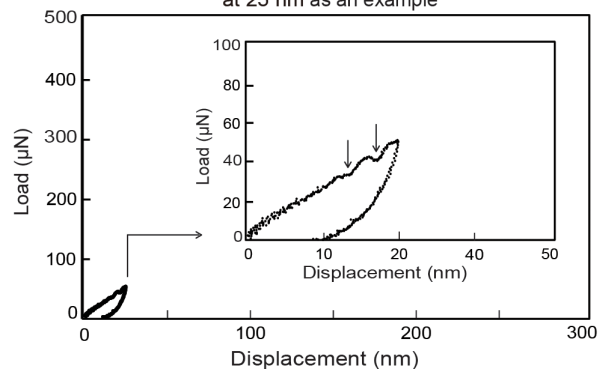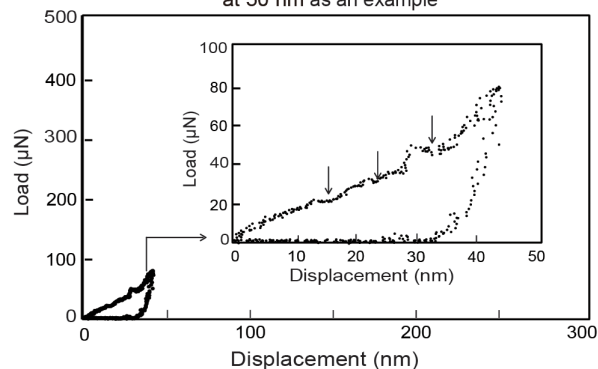
Figure 6 | Compression load displacement curves for displacements of 25 nm, 50 nm and 75 nm for CNHs with the vertical arrows showing examples of pop-in events. Here pop-in events are a result from buckling of individual nanohorns.

For indentation with a sharp tip, the load-displacement curves revealed several pop-in effects which results as the sharp tip penetrates broken layers and spaces between separated layers. The hardness of the MoS_2 MWNTs was found to be similar to bulk and does not follow a smaller is stronger trend. Separated layers, broken layers, and missing layers and Shockley dislocations decrease resistance to deformation and compete with Frank dislocations present which increase resistance to deformation. This results in no appreciable change in hardness. For compression, pop-in effects from the sudden displacement of material were observed in both MWNTs during loading similar to nanoindentation for MWNTs. For CNHs pop-ins were also observed and resulted from buckling of the horns of the nanoparticle. The defected layers of MoS_2 MWNTs and the
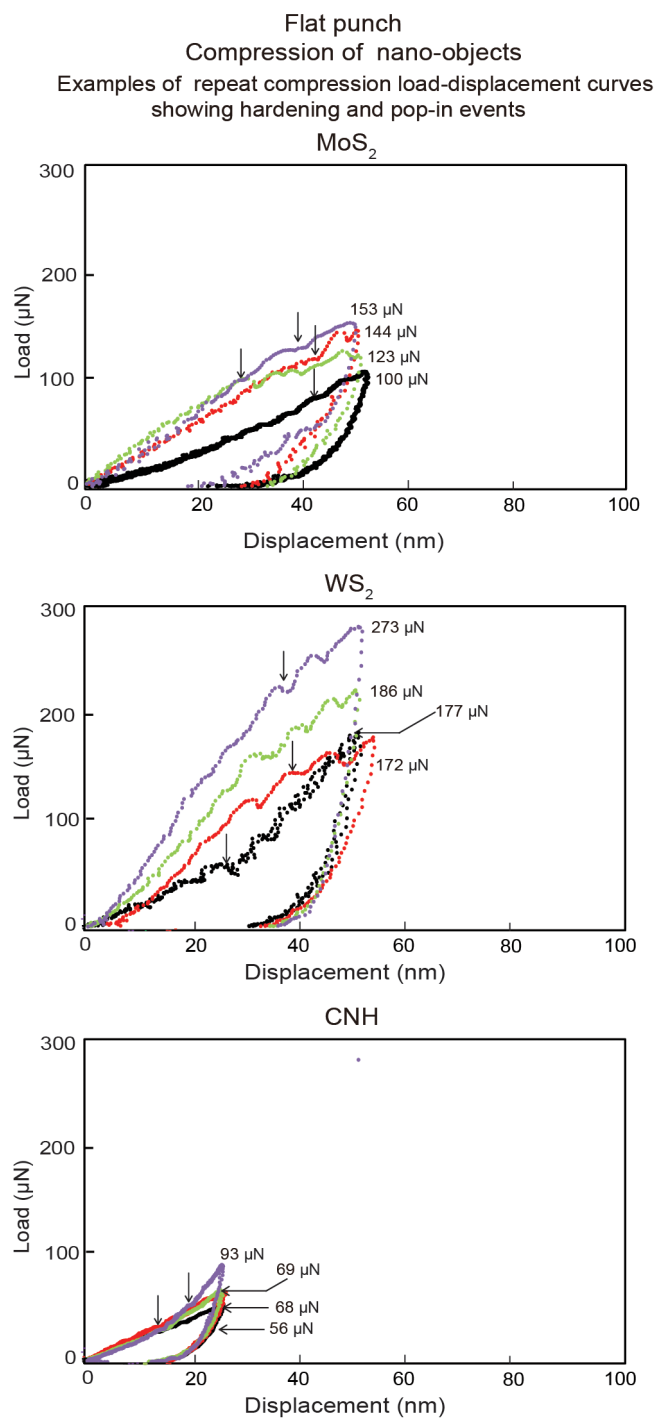
Figure 7 | Examples of repeat load-displacement curves for MoS₂ and WS₂ MWNTs at a constant displacement of 50 nm and CNHs at a constant displacement of 25 nm. Vertical arrows point to pop-in events. Pop-in events for the nanotubes occur due to breaking of walls, and sudden compression of separated layers. For the CNH nanoparticle pop-in events occur due to buckling of individual nanohorns. Evidence hardening can be seen for all three cases where the loads increase at a constant displacement.

flexibility of the graphene results in less resistance to deformation compared to WS₂ MWNTs which do not show separated and broken layers observed in MoS₂ MWNTs. Repeat compression tests showed a hardening effect with each subsequent load at constant displacement. The resulting load for constant displacement was either the same or higher than the previous. For the nanotubes, this was due to

increased resistance to deformation as a result of the layers of the nanotubes being pressed together. For the CNHs, individual horns buckle and are pressed against each other and onto the substrate making further compression more difficult.

All three nano-objects display pop-in effect during loading and increased resistance to deformation during repeat compression tests. CNHs required the smallest load for a displacement of 50 nm compared to the MWNTs. This is due to buckling of the individual nano-horns as a result of their flexible nature.

Deformation studies comparing local deformation (indentation) and global deformation (compression) on the nanoscale to examine scale effects of mechanical properties and deformation mechanisms of MoS₂ MWNTs was performed. Global deformation studies onWS₂ MWNTs and carbon nanohorns were also performed. These studies aid in understanding how nano-objects and materials behave during loading and unloading in tribological applications.

The knowledge gained will have far reaching effects when designing macro-to nanoscale systems that incorporate materials with nano-dimensions for reducing friction and wear.

1. Duncan, R. The dawning era of polymer therapeutics. *Nat. Rev. Drug Discov.* **2**, 347–360 (2003).
2. Murakami, T. *et al.* Drug-Loaded Carbon Nanohorns: Adsorption and Release of Dexamethasone in Vitro. *Mol. Pharmaceutics* **1**, 399–405 (2004).
3. Ferrari, M. Cancer nanotechnology: opportunities and challenges. *Nat. Rev. Cancer* **5**, 161–171 (2005).
4. Panyala, N. R., Pena-Mendez, E. M. & Havel, J. Gold and nano-gold in medicine: overview, toxicology and perspectives. *J. Appl. Biomed.* **7**, 75–91 (2009).
5. Berlin, J. M. *et al.* Engineered nanoparticles for hydrocarbon detection in oil-field rocks. *Energy Environ. Sci.* **4**, 505–509 (2011).
6. Matteo, C., Candido, P., Vera, R. & Francesca, V. Current and future nanotech applications in the oil industry. *Am. J. Appl. Sci.* **9**, 784–793 (2012).
7. Ryoo, S. *et al.* Theoretical and experimental investigation of the motion of multiphase fluids containing paramagnetic nanoparticles in porous media. *J. Petrol. Sci. and Eng.* **81**, 129–144 (2012).
8. Thanikaivelan, P., Narayanan, N. T., Pradhan, B. K. & Ajayan, P. M. Collagen based magnetic nanocomposites for oil removal applications. *Sci. Rep.* **2**, doi:10.1038/srep00230 (2012).
9. Pavía-Sanders, A. *et al.* Robust magnetic/polymer hybrid nanoparticles designed for crude oil entrapment and recovery in aqueous environments. *ACS Nano* **7**, 7552–7561 (2013).
10. Bhushan, B. & Gupta, B. K. *Handbook of tribology: materials, coatings, and surface treatments* (McGraw-Hill, New York, 1991).
11. Rapoport, L. *et al.* Slow Release of Fullerene-Like WS₂ Nanoparticles as a Superior Solid Lubrication Mechanism in Composite Matrices. *Adv. Eng. Mater.* **3**, 71–75 (2001).
12. Rapoport, L. *et al.* Friction and wear of fullerene-like WS₂ under severe contact conditions: friction of ceramic materials. *Tribol. Lett.* **19**, 143–149 (2005).
13. Tanaka, A. *et al.* Friction and Wear of Carbon Nanohorn-Containing Polyimide Composites. *Tribol. Lett.* **19**, 135–42 (2005).
14. St. Dennis, J. E., Jin, K., John, V. T. & Pesika, N. S. Carbon Microspheres as Ball Bearings in Aqueous-Based Lubrication. *ACS Appl. Mater. Interfaces* **3**, 2215–2218 (2011).
15. Maharaj, D. & Bhushan, B. Effect of spherical Au nanoparticles on nanofriction and wear reduction in dry and liquid environments. *Beilstein J. Nanotechnol.* **3**, 759–772 (2012).
16. Maharaj, D. & Bhushan, B. Effect of MoS₂ and WS₂ nanotubes on nanofriction and wear reduction in dry and liquid environments. *Tribol. Lett.* **49**, 323–339 (2013).
17. Maharaj, D., Bhushan, B. & Iijima, S. Effect of Carbon Nanohorns on nanofriction and wear reduction in dry and liquid environments. *J. Colloid Interface Sci.* **400**, 147–160 (2013).
18. Akbulut, M., Belman, N., Golan, Y. & Israelachvili, J. Frictional Properties of Confined Nanorods. *Adv. Mater.* **18**, 2589–2592 (2006).
19. Singh, D. P., Polychronopoulou, K., Rebholz, C. & Aouadi, S. M. Room temperature synthesis and high temperature frictional study of silver vanadate nanorods. *Nanotechnology* **21**, 325601 (2010).
20. Zhang, J. & Zhang, J. Surfactant Inducing Phase Change of ZnO Nanorods to Low Friction. *Tribo. Lett.* **49**, 77–83 (2013).
21. Lüthi, R. *et al.* Sled-Type Motion on the Nanometer Scale: Determination of Dissipation and Cohesive Energies of C60. *Science* **266**, 1979–1981 (1994).
22. Sitti, M. Atomic force microscope probe based controlled pushing for nanotribological characterization. *IEEE/ASME Trans. Mechatronics* **9**, 343–349 (2004).

23. Ritter, C., Heyde, M., Stegemann, B., Rademann, K. & Schwarz, U. D. Contact-area dependence of frictional forces: Moving adsorbed antimony nanoparticles. *Phys. Rev. B* **71**, 085405 (2005).
24. Dietzel, D. *et al.* Interfacial friction obtained by lateral manipulation of nanoparticles using atomic force microscopy techniques. *J. Appl. Phys.* **102**, 084306 (2007).
25. Palacio, M. & Bhushan, B. A nanoscale friction investigation during manipulation of nanoparticles in controlled environments. *Nanotechnology* **19**, 315710 (2008).
26. Lahouij, I., Dassenoy, F., de Knoop, L., Martin, J.-M. & Vacher, B. In Situ TEM Observation of the Behavior of an Individual Fullerene-Like MoS2 Nanoparticle in a Dynamic Contact. *Tribol. Lett.* **42**, 133–140 (2011).
27. Tevet, O. *et al.* Friction mechanism of individual multilayered nanoparticles. *Proc. Natl. Acad. Sci. U S A* **108**, 19901–19906 (2011).
28. Kalin, M., Kogovšek, J. & Remškar, M. Mechanisms and improvements in the friction and wear behavior using MoS₂ nanotubes as potential oil additives. *Wear* **280–281**, 36–45 (2012).
29. Maharaj, D. & Bhushan, B. Nanomanipulation, nanotribology and nanomechanics of Au nanorods in dry and liquid environments using an AFM and depth sensing nanoindenter. *Nanoscale* **6**, 5838–5852 (2014a).
30. Bhushan, B. Introduction to Tribology, 4th ed., (Wiley, New York, 2013).
31. Anonymous, Standard test method for microhardness of materials [359–379] (ASME, New York, 1979).
32. Iijima, S. *et al.* Nano-aggregates of single-walled graphitic carbon nano-horns. *Chem. Phys. Lett.* **309**, 165–170 (1999).
33. Kasuya, D., Yudasaka, M., Takahashi, K., Kokai, F. & Iijima, S. Selective Production of Single-Wall Carbon Nanohorn Aggregates and Their Formation Mechanism. *J. Phys. Chem. B* **106**, 4947–51 (2002).
34. Oliver, W. C. & Pharr, G. M. An improved technique for determining hardness and elastic modulus using load and displacement sensing indentation experiments. *J. Mat. Res.* **7**, 1564–1583 (1992).
35. Harper, C. A. *Handbook of Ceramics, Glasses and Diamonds* (McGraw-Hill, New York, 2001).
36. Feldman, J. L. Elastic constants of 2H-MoS2 and 2H-NbSe2 extracted from measured dispersion curves and linear compressibilities. *J. Phys. Chem. Solids* **37**, 1141–1144 (1976).
37. Hull, D. & Bacon, D. J. *Introduction to dislocations* (Butterworth-Heinemann, Woburn, Massachusetts 2001).
38. Goken, M. & Kempf, M. Pop-ins in nanoindentation – The initial yield point. *Z. Metallkd.* **92**, 1061–1067 (2001).
39. Lee, C., Wei, X., Kysar, J. W. & Hone, J. Measurement of the Elastic Properties and Intrinsic Strength of Monolayer Graphene. *Science* **321**, 385–388 (2008).
40. Zhang, Y. & Pan, C. Measurements of mechanical properties and number of layers of graphene from nano-indentation. *Diam. Relat. Mater.* **24**, 1–5 (2012).
41. Wakabayashi, N., Smith, H. G. & Nicklow, R. M. Lattice dynamics of hexagonal Mo studied by neutron scattering. *Phys. Rev. B* **12**, 659–663 (1975).
42. Thilly, L., Lecouturier, F. & von Stebut, J. Size-induced enhanced mechanical properties of nanocomposite copper/niobium wires: nanoindentation study. *Acta Mater.* **51**, 5049–5065 (2003).
43. Greer, J. R., Oliver, W. C. & Nix, W. D. Size dependence of mechanical properties of gold at the micron scale in the absence of strain gradients. *Acta Mater.* **53**, 1821–1830 (2005).
44. Wu, B., Heidelberg, A. & Boland, J. J. Mechanical properties of ultrahigh-strength gold nanowires. *Nature Mater.* **4**, 525–552 (2005).
45. Shan, Z. W., Mishra, R. K., Asif, S. A. S., Warren, O. L. & Minor, A. M. Mechanical annealing and source-limited deformation in submicrometer-diameter Ni crystals. *Nature Mater.* **7**, 115–119 (2008).
46. Dietiker, M., Buzzi, S., Pigozzi, G., Löffler, J. F. & Spolenak, R. Deformation behavior of gold nano-pillars prepared by nanoimprinting and focused ion-beam milling. *Acta Mater.* **59**, 2180–2192 (2011).
47. Mordehai, D. *et al.* Size effect in compression of single-crystal gold microparticles. *Acta Mater.* **59**, 5202–5215 (2011).
48. Maharaj, D. & Bhushan, B. Scale effects of nanomechanical properties and deformation behavior of Au nanoparticle and thin film using depth sensing nanoindentation. *Beilstein J. Nanotechnol.* **5**, 822–836 (2014).
49. Li, J. C. M. Pile-up of dissociated dislocations and the strength-grain size relationship. *Philos. Mag.* **19**, 189–198 (1969).
50. Ashby, M. F. The deformation of plastically non-homogeneous materials. *Philos. Mag.* **21**, 399–424 (1970).
51. Gracio, J. J. The double effect of grain size on the work hardening behaviour of polycrystalline copper. *Scripta Metall. Mater.* **31**, 487–489 (1994).
52. Conrad, H. & Jung, K. Effect of grain size from millimeters to nanometers on the flow stress and deformation kinetics of Ag. *Mat. Sci. Eng. A* **391**, 272–284 (2005).
53. Pope, L. E. & Panitz, J. K. G. The effects of hertzian stress and test atmosphere on the friction coefficients of MoS2 coatings. *Surf. and Coat. Tech.* **36**, 341–350 (1988).
54. Uemura, M., Saito, K. & Nakao, K. A Mechanism of Vapor Effect on Friction Coefficient of Molybdenum Disulfide. *Tribol. Trans.* **33**, 551–556 (1990).
55. Prasad, S. V. & Zabinski, J. S. Tribology of tungsten disulfide (WS2) – characterization of wear –induced transfer films. *J. Mater. Sci. Lett.* **12**, 1413–1415 (1993).
56. Scarpa, F., Adhikari, S. & Phani, A. S. Effective elastic mechanical properties of single layer graphene sheets. *Nanotechnol.* **20**, 065709 (2009).

Acknowledgments

Author contributions

D.M. performed the experiments and analyzed the data. D.M. wrote the main text and D.M. and B.B. participated equally in planning, execution, and review of the manuscript.

Additional information

Competing financial interests: The authors declare no competing financial interests.

How to cite this article: Maharaj, D. & Bhushan, B. Nanomechanical behavior of MoS₂ and WS₂ multi-walled nanotubes and Carbon nanohorns. *Sci. Rep.* **5**, 8539; DOI:10.1038/srep08539 (2015).